



Direct aerosol chemical composition measurements to evaluate the physicochemical differences between controlled sea spray aerosol generation schemes

D. B. Collins^{1,***}, D. F. Zhao^{1,*,***}, M. J. Ruppel¹, O. Laskina², J. R. Grandquist², R. L. Modini^{3,**}, M. D. Stokes³, L. M. Russell³, T. H. Bertram¹, V. H. Grassian², G. B. Deane³, and K. A. Prather^{1,3}

¹Department of Chemistry and Biochemistry, University of California, San Diego, La Jolla, CA 92093, USA

²Department of Chemistry, University of Iowa, Iowa City, IA 52242, USA

³Scripps Institution of Oceanography, University of California, San Diego, La Jolla, CA 92093, USA

* now at: Institute of Energy and Climate Research, IEK-8: Troposphere, Forschungszentrum Jülich GmbH, 52425 Jülich, Germany

** now at: École Polytechnique Fédérale de Lausanne (EPFL), 1015 Lausanne, Switzerland

***These authors contributed equally to this work.

Correspondence to: K. A. Prather (kprather@ucsd.edu)

Received: 4 June 2014 – Published in Atmos. Meas. Tech. Discuss.: 3 July 2014

Revised: 26 September 2014 – Accepted: 29 September 2014 – Published: 6 November 2014

Abstract. Controlled laboratory studies of the physical and chemical properties of sea spray aerosol (SSA) must be underpinned by a physically and chemically accurate representation of the bubble-mediated production of nascent SSA particles. Bubble bursting is sensitive to the physicochemical properties of seawater. For a sample of seawater, any important differences in the SSA production mechanism are projected into the composition of the aerosol particles produced. Using direct chemical measurements of SSA at the single-particle level, this study presents an intercomparison of three laboratory-based, bubble-mediated SSA production schemes: gas forced through submerged sintered glass filters (“frits”), a pulsed plunging-waterfall apparatus, and breaking waves in a wave channel filled with natural seawater. The size-resolved chemical composition of SSA particles produced by breaking waves is more similar to particles produced by the plunging waterfall than those produced by sintered glass filters. Aerosol generated by disintegrating foam produced by sintered glass filters contained a larger fraction of organic-enriched particles and a different size-resolved elemental composition, especially in the 0.8–2 μm dry diameter range. Interestingly, chemical differences between the methods only emerged when the particles were chemically analyzed at the single-particle level as a function of size;

averaging the elemental composition of all particles across all sizes masked the differences between the SSA samples. When dried, SSA generated by the sintered glass filters had the highest fraction of particles with spherical morphology compared to the more cubic structure expected for pure NaCl particles produced when the particle contains relatively little organic carbon. In addition to an intercomparison of three SSA production methods, the role of the episodic or “pulsed” nature of the waterfall method on SSA composition was undertaken. In organic-enriched seawater, the continuous operation of the plunging waterfall resulted in the accumulation of surface foam and an over-expression of organic matter in SSA particles compared to those produced by a pulsed plunging waterfall. Throughout this set of experiments, comparative differences in the SSA number size distribution were coincident with differences in aerosol particle composition, indicating that the production mechanism of SSA exerts important controls on both the physical and chemical properties of the resulting aerosol with respect to both the internal and external mixing state of particles. This study provides insight into the inextricable physicochemical differences between each of the bubble-mediated SSA generation mechanisms tested and the aerosol particles that they produce, and

also serves as a guideline for future laboratory studies of SSA particles.

1 Introduction

Understanding the production and characteristics of natural atmospheric aerosol particles is critical for constraining their influence on our global climate (e.g., Charlson et al., 1992; Ramanathan et al., 2001; Menon et al., 2002; Lohmann and Feichter, 2005; Carslaw et al., 2013; Ghan et al., 2013; Tsigaridis et al., 2013) and for the accurate prediction of chemical processes in the atmosphere (Andreae and Crutzen, 1997; Brown and Stutz, 2012). Sea spray aerosol (SSA) particles, which are ejected from the ocean surface through the disintegration of whitecap foam (Blanchard and Woodcock, 1957; Lewis and Schwartz, 2004; de Leeuw et al., 2011), represent one of the most dominant types of natural atmospheric aerosol (Andreae and Rosenfeld, 2008). The production flux and physicochemical properties of SSA that are emitted over the wide range of possible oceanic conditions are not sufficiently constrained for proper inclusion in climate models (Lewis and Schwartz, 2004; de Leeuw et al., 2011; Quinn and Bates, 2011; Gantt and Meskhidze, 2013; Tsigaridis et al., 2013).

While SSA has long been known to consist of both inorganic salts and organic material (Blanchard, 1964; Duce and Hoffman, 1976; Novakov et al., 1997), field studies during the past decade have suggested that the organic fraction of marine aerosol is enhanced when the particles are ejected from seawater that is host to elevated biological activity (e.g., O'Dowd et al., 2004). Seasonal trends in organic aerosol mass supporting the influence of biological activity on SSA composition have been observed in the northern and southern midlatitudes (Yoon et al., 2007; Sciare et al., 2009), but ambient studies cannot always unambiguously assign changes in the composition of SSA to specific primary, secondary, anthropogenic, and/or continental sources (Sorooshian et al., 2009; Shank et al., 2012).

Laboratory studies are quite commonly conducted to generate and study nascent SSA that is uncontaminated by particles found in the marine boundary layer that are produced by other sources. These studies produce SSA from disintegrating foam in natural seawater or proxy materials mainly by means of sintered glass bubblers or plunging water jets. (Sellegri et al., 2006; Keene et al., 2007; Tyree et al., 2007; Fuentes et al., 2010b; Hultin et al., 2010; Bates et al., 2012; Park et al., 2014). Since it is well known that SSA is produced by the bursting of air bubbles at the sea surface (e.g., Blanchard and Woodcock, 1957; Lewis and Schwartz, 2004; de Leeuw et al., 2011), the differences between generation methods for SSA in the laboratory differ primarily by the method of bubble production. Recent reports indicate that pneumatic atomization does not produce particles of similar physical or chemical properties to those generated by bubble

bursting (Fuentes et al., 2010b; Gaston et al., 2011). Until recently, two different bubble production techniques have been utilized for laboratory studies of aerosol composition: (1) air (or N₂) forced through sintered glass filters (“frits”) (Cloke et al., 1991; Keene et al., 2007; Wise et al., 2009; Fuentes et al., 2010b; Modini et al., 2010; Park et al., 2014), and (2) impinging water jets (Facchini et al., 2008; Fuentes et al., 2010b; Hultin et al., 2010). A new approach introduced by Prather et al. (2013) produces SSA using reproducible breaking waves in a linear wave channel filled with natural, filtered seawater. While laboratory waves may not reproduce all of the factors that lead to SSA production over the ocean, they do produce bubble size distributions that compare favorably with those measured in whitecaps (Deane and Stokes, 2002). Consequently, aerosol generation by means of the wave-breaking method provides the closest proxy to natural SSA currently available in a controlled environment.

Experiments to compare the characteristics of aerosols produced using sintered glass filters, plunging water jets or waterfalls, and breaking waves have shown that each has a distinctly different and characteristic size distribution (Sellegri et al., 2006; Fuentes et al., 2010b; Prather et al., 2013; Stokes et al., 2013). Some intercomparison studies have investigated water uptake properties of the aerosol as indirect measures of composition (Fuentes et al., 2010b; King et al., 2012); however, the findings of each study depend on the specific operating conditions of each bubble-mediated aerosol generation method tested. In this study, direct chemical measurements of SSA generated using sintered glass filters and a plunging waterfall were compared against SSA produced by laboratory breaking waves to investigate the importance of reproducing various physical elements of the wave-breaking process in the generation of nascent SSA in the laboratory. The impact of continuous bubble production, which can result in the accumulation of foam at the water surface several bubble layers thick, on the composition of SSA is also discussed.

2 Experimental methods

Two sets of experiments were conducted: (1) the intercomparison experiments to compare the production of SSA between sintered glass filters, a plunging waterfall, and breaking waves, and (2) the foam production experiments to study the effects of pulsed versus continuous foam production. The intercomparison experiments were staged in the glass-walled wave channel in the Scripps Institution of Oceanography (SIO) Hydraulics Laboratory, while the foam production experiments were carried out using a Marine Aerosol Reference Tank. Both studies are described below.

2.1 Sea spray generation methods intercomparison

Sea spray aerosol particles were generated using sintered glass filters, a plunging waterfall, and breaking waves in a 33 m × 0.5 m × 0.6 m (length–width–water depth, 9900 L) glass-walled wave channel managed by the Hydraulics Laboratory at SIO, which has been recently adapted for ocean–atmosphere interaction studies (Prather et al., 2013), and is shown schematically in Fig. 1. Prior to each experiment, the wave channel was filled with natural, coastal seawater from 275 m offshore and approximately 4 m below the low-tide line at the SIO Pier (La Jolla, CA; 32°52.0′ N, 117°15.4′ W). Detailed information on the seawater delivery system to the wave channel facility is provided by Prather et al. (2013). All SSA generation methods tested in these intercomparison experiments were operated using the same sample of seawater within 24 h of filling the wave channel to ensure that the biogeochemical state of the seawater closely represented the natural seawater supply and chemical changes in the seawater itself were minimized. Sweep air that was filtered and scrubbed of reactive trace gases was supplied to the wave channel headspace continuously with a linear velocity of approximately 6 cm s⁻¹. Bubbles were generated using each of the three methods approximately 1 m upstream of the sampling manifold, giving a particle residence time in the headspace of the wave channel of approximately 17 s.

2.1.1 Controlled breaking waves

Individual breaking waves were generated by a computer-controlled hydraulic paddle. The breaking waves were formed when a train of wave pulses of varying amplitude and speed generated at one end of the channel were focused and superimposed to form a plunging breaker at a set location along the wave channel's long axis. This hydraulic-paddle-induced wave production at the SIO Hydraulics Laboratory wave channel facility is described in detail elsewhere (Deane and Stokes, 2002; Callaghan et al., 2013). Waves were generated with a maximum frequency of 1 min⁻¹. Bubbles entrained in the water column by the wave-breaking event penetrated to approximately 15 cm below the water surface. The lack of background particle contamination was verified every 5 min by generating a wave pulse train with an amplitude insufficient to induce a wave-breaking event to ensure that the wave generation mechanism did not contaminate the sample.

2.1.2 Plunging waterfall

Specifically designed as a physical mimic to wave breaking, a plunging-waterfall apparatus was implemented to generate aerosol in the same location of the wave channel where wave breaking occurs. In this technique, seawater was recirculated from the wave channel through a centrifugal pump to a horizontal slotted cylinder approximately 40 cm above the wa-

ter surface. The recirculating flow to the waterfall apparatus was modulated with a 6 s on/6 s off cycle that allowed the foam patch at the waterfall impinging location to decay before plunging resumed. As a result of the modulated flow, the waterfall swept across a 30 cm × 50 cm patch of the wave channel surface, disturbing the surface and forming bubbles throughout the swept area. This system is based on the same design criteria used to engineer the plunging-waterfall system in the Marine Aerosol Reference Tank described by Stokes et al. (2013).

2.1.3 Sintered glass filters

The setup utilized in this intercomparison was similar to that implemented by Keene et al. (2007) and is identical to that utilized by Prather et al. (2013). The distance from the top of the sintered glass filter, where bubbles are released into the water, to the water surface was approximately 35 cm, which is smaller than the 115 cm rise distance used by Keene et al. (2007). Nitrogen gas was forced through two sintered glass filters of porosity “A” (145–174 μm pore diameter) and four of porosity “E” (4–8 μm pore diameter). Each set of glass filters of a particular porosity was supplied a total of 0.5 L per minute N₂ gas, so that the gas flux for the two sets of bubble sizes was equal.

2.2 Foam production experiments

The impact of standing foam on SSA composition was investigated using the plunging-waterfall mechanism in a Marine Aerosol Reference Tank (MART) system (Stokes et al., 2013). The plunging waterfall utilized in the intercomparison experiment performed in the wave channel (Sect. 2.1.2) is mechanistically similar to the aerosol generation system implemented in the MART. The plunging waterfall was operated in two modes: “continuous” and “pulsed”. While in “continuous” mode, the waterfall was continuously generated by recirculating water from the bottom of the tank to the waterfall apparatus suspended above the water surface through a centrifugal pump. In “pulsed” mode, the recirculation flow to the waterfall apparatus was modulated with a 4 s on, 4 s off pattern. During the “on” cycle, the flow rate of water was approximately 40 L per minute.

Seawater for MART-based experiments was collected from the ocean surface 275 m offshore at the end of Scripps Pier, from a more shallow depth than the source of seawater used in the intercomparison experiments. Results utilizing this unaltered seawater condition are labeled “natural seawater” in Sect. 3.2. In order to perform this foam production experiment with high organic matter concentrations, the natural seawater sample was augmented with Guillard's f/2 media (including 13 mg L Na₂SiO₃; Aquatic EcoSystems, Inc., Apopka, FL) and was continuously supplied with cool white light (~100 μE m⁻², 6500 K; Phillips Alto II, F32T8/DX), allowing for an unconstrained phytoplankton bloom to take

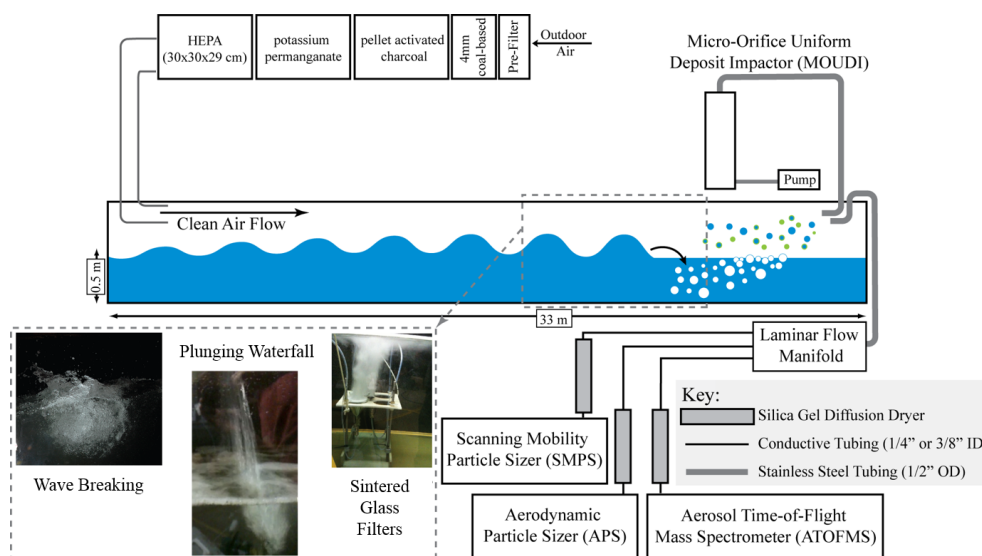


Figure 1. Schematic of the linear wave channel with interchangeable bubble generation apparatuses for SSA production. Each of these bubble generation mechanisms were tested within the wave channel within 24 hours, and with the same natural seawater sample.

place over the course of 1 to 2 weeks, in which the large majority of the autotrophic biomass consisted of diatoms. Proliferation of heterotrophic bacteria was observed upon phytoplankton senescence in agreement with the canonical view of biological processes active within the microbial loop (Pomeroy et al., 2007). Chlorophyll *a* concentrations reached as high as 140 mg m^{-3} and then subsided to 20 mg m^{-3} , at which time the foam production experiments were conducted (Sect. 3.2). Autotrophic organisms, the abundance of which is indicated through the chlorophyll *a* concentration, are well known to exude organic material, increasing the organic matter concentration in the seawater throughout the bloom lifetime. Heterotrophic organisms (e.g., bacteria, grazers) then process these organic exudates (Ogawa et al., 2001; Teeling et al., 2012), chemically altering the dissolved organic matter produced by the autotrophic biomass. This method of enriching the seawater with organic matter allows for natural dynamic ecosystem processes to shape the composition of the organic matter in the seawater, similar to the types of interactions found in natural phytoplankton blooms (Azam and Malfatti, 2007; Pomeroy et al., 2007; Teeling et al., 2012). While the total chlorophyll *a* concentration in these experiments is an indirect indicator of the autotrophic biomass, it is notable that various controlled SSA generation studies have shown that the amount of organic matter imparted to SSA is only a weak function of the seawater chlorophyll concentration, and depends instead on the amount and composition of organic matter in the seawater (Ault et al., 2013; Collins et al., 2013; Prather et al., 2013; Park et al., 2014; Quinn et al., 2014). Total organic carbon (TOC) concentrations in the seawater were measured by means of the high temperature combustion method (Shimadzu Scientific Instruments) after acidifying the sample with 12N hydrochloric acid. While the

exact molecular identity of the organic compounds in the seawater in these experiments was not known, the composition of the seawater utilized in this experiment can be reasonably expected to be more chemically similar to regions of the ocean that are naturally organic-matter-enriched than a salt water mixture doped with organic proxy molecules. This experiment therefore also benefits from naturally accurate influences of organic matter physicochemical properties on bubble physics and sea surface microlayer properties.

2.3 Aerosol measurements

All aerosol measurements were conducted after passing the sample through silica gel diffusion driers to attain a relative humidity $< 15\%$. Number size distributions of aerosol particles were measured using a scanning mobility particle sizer (SMPS) for particles with mobility diameters (d_m) between 0.013 and $0.7 \mu\text{m}$, and an aerodynamic particle sizer (APS) for particles with aerodynamic diameters (d_a) between 0.6 and $20 \mu\text{m}$. Size distributions from these two different instruments with different size metrics were unified by converting both d_m and d_a to the physical diameter (d_p) according to Eqs. (1) and (2) (DeCarlo et al., 2004), assuming all particles were spherical and had a density (ρ_p) of 1.8 g cm^{-3} (Zelenyuk et al., 2007) and a reference density (ρ_0) of 1 g cm^{-3} .

$$d_p = d_m \quad (1)$$

$$d_p = d_a \left(\frac{\rho_0}{\rho_p} \right)^{1/2} \quad (2)$$

Since particles were dried prior to sampling, the spherical particle assumption may not be accurate in all cases. Assuming all particles were cubic would decrease d_p derived from

d_m by 8 %, and would increase d_p derived from d_a by 4 % (DeCarlo et al., 2004). SSA is an external mixture of particles with different compositions and physicochemical properties (Collins et al., 2013; Prather et al., 2013), including size-dependent differences in morphology (Ault et al., 2013). Caution is therefore encouraged when making quantitative comparisons between SSA size distributions reported using different methods.

The size-resolved chemical composition of SSA was characterized by aerosol time-of-flight mass spectrometry (ATOFMS). Two ATOFMS instruments were used in parallel: one was fitted with a converging nozzle inlet (Gard et al., 1997) and measured particles with vacuum aerodynamic diameters (d_{va}) between 0.5 and 3 μm , while a second, using an aerodynamic lens inlet (Su et al., 2004), measured particles with d_{va} between 0.1 and 2.5 μm . In both ATOFMS instruments, particles transmitted through the inlet reach a size-dependent terminal velocity in a differentially pumped vacuum chamber, where they intersect two continuous wave lasers (532 nm; 50 mW) positioned at a fixed distance along the flight trajectory. The light scattered as the particle intersects each beam is collected and the time between each set of light scatter pulses is used to determine the velocity of each particle. Particle velocities are translated to d_{va} using a calibration curve generated using polystyrene latex (PSL) spheres of known diameter (density = 1.05 g cm⁻³). In order to make convenient correspondence with the number size distributions presented herein, d_{va} was converted to d_p using the density of PSL in this case for ρ_0 (Eq. 3); however, caution in making comparisons is again encouraged due to the inherent morphology and density assumptions required for conversions between size metrics.

$$d_p = d_{va} \frac{\rho_0}{\rho_p} \quad (3)$$

The measured particle velocity is also used to trigger a pulsed, Q-switched Nd:YAG laser (266 nm; 1.3 mJ; 7 ns) that intersects each particle in the ion source region of the mass spectrometer, where particle desorption and ionization occur using a single laser pulse. Positive and negative ion time-of-flight mass spectra are obtained for each particle. Information about the ATOFMS is provided in greater detail in prior publications (Gard et al., 1997; Su et al., 2004). ATOFMS data were post-processed using the YAADA toolkit (<http://www.yaada.org>) for Matlab (The MathWorks Inc.). Particles were classified according to their mass spectral signatures using a neural network algorithm, Art-2a (Song et al., 1999), with a vigilance factor of 0.85 and a learning rate of 0.05. The resulting clusters were refined by computationally regrouping with a threshold of 0.90. Five distinct particle types (Fig. 2) were formed by manually grouping Art-2a classes based on their characteristic mass spectra based on the classifications described by Prather et al. (2013).

In addition to in situ single-particle composition measurements using ATOFMS, SSA samples were collected for

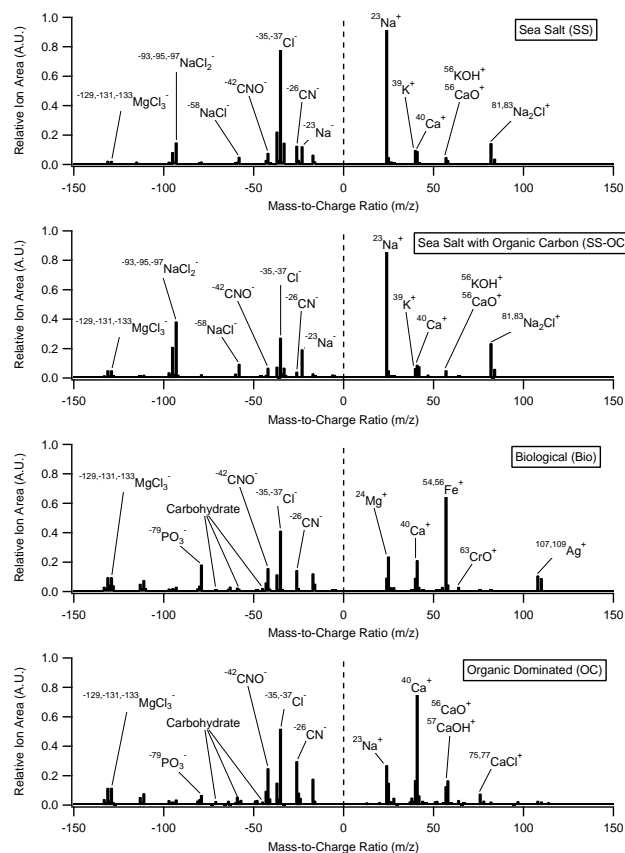


Figure 2. Representative mass spectra for each of the particle types described in this study.

offline analysis by scanning electron microscopy (SEM). Aerosol samples were deposited on silicon wafer substrates using a micro-orifice uniform deposit impactor (MOUDI; MSP Corporation). SEM images were collected using a Hitachi S-4800 scanning electron microscope with a 5 kV accelerating voltage and a 9.2–9.6 mm working distance. Single-particle analysis was performed using computer-controlled SEM combined with an IXRF Systems energy dispersive X-ray (EDX) spectrometer (CCSEM/EDX). EDX data were analyzed with Iridium Ultra software (IXRF Systems) for automated particle analysis. The computer-controlled system analyzes the sample on a field-by-field basis. Once particles are identified in a field of view, the software acquires an X-ray spectrum for each particle. X-ray spectra were acquired for 20 s at a beam current of 15 μA and an accelerating voltage of 5 kV. Particle size was determined by automated measurement of the area of each particle. The area-equivalent diameter (d_{ae}) was then calculated using Eq. (4):

$$d_{ae} = \left(\frac{4A}{\pi} \right)^{1/2}, \quad (4)$$

Table 1. Tabulated number of particles analyzed by SEM-EDX in each size bin.

d_{ae} (μm)	Sintered glass filters	Plunging waterfall	Wave breaking
0.3–0.4	166	171	54
0.4–0.5	76	75	41
0.5–0.6	29	42	37
0.6–0.7	17	37	31
0.7–0.8	13	49	28
0.8–0.9	38	48	32
0.9–1.0	31	29	27
1.0–1.1	35	38	28
1.1–1.2	25	29	25
1.2–1.3	20	41	22
1.3–1.4	14	44	26
1.4–1.5	11	45	30
1.5–1.7	16	59	45
1.7–1.9	33	62	27
1.9–2.1	26	52	33
2.1–2.3	20	36	17
2.3–2.5	18	19	13
2.5–2.7	23	13	9
2.7–3.0	17	5	6
Total 0.3–3.0	678	963	546

where A is the geometric area of the particle in the image. Conversion of area equivalent diameter to physical diameter for particles deposited on MOUDI substrates are associated with an uncertainty in particle shape. The shape of particles deposited on a substrate depends on viscosity and surface tension (O'Brien et al., 2014), neither of which are known for SSA. Consequently, particle sizes within the CCSEM/EDX analysis were not converted to d_p .

In total, 2187 particles with d_{ae} between 0.3 and 3 μm were analyzed. Any particle intersected by the boundary of the image was neglected to ensure that only particles that were completely imaged are included in the analysis. All measured particles were segregated into size bins for analysis. The number of particles analyzed in each size bin for each aerosol generation method can be found in Table 1.

3 Results

3.1 SSA generation method intercomparison

The physicochemical properties of SSA particles have been associated with the physical characteristics of bubbles in many prior publications (e.g., Blanchard and Woodcock, 1957; Lewis and Schwartz, 2004; Sellegri et al., 2006; Fuentes et al., 2010b; de Leeuw et al., 2011; King et al., 2012); however, direct comparison with SSA produced by a breaking wave in the laboratory, assumed to be a good proxy

for nascent sea spray, has only recently been realized (Prather et al., 2013). The physicochemical characteristics of aerosol production from bubble bursting have been linked not only to the size distribution of SSA (Sellegri et al., 2006; Fuentes et al., 2010b; Zabori et al., 2012) but also to the water uptake properties of SSA particles (Fuentes et al., 2010b; King et al., 2012). This study extends prior investigations by directly probing the influence of bubble-bursting mechanisms on the detailed composition of SSA particles using direct chemical measurements at the single-particle level.

As discussed earlier, aerosol particles were generated using breaking waves, a plunging waterfall, and sintered glass filters in natural seawater. The laboratory breaking waves used here have bubble size distributions that are representative of those observed in open-ocean waves (Deane and Stokes, 2002) and particles from the breaking waves are taken to be the best proxy for oceanic SSA. As discussed by Prather et al. (2013), the number size distribution of SSA particles derived from sintered glass filters had a modal diameter of approximately 60 nm, whereas the plunging waterfall and wave-breaking particles exhibit modal diameters of approximately 190 and 200 nm, respectively (Fig. 3b). The differences in size distribution shape and modal diameter suggest that the dominant SSA production mechanism of SSA from the sintered glass filters could be different from SSA produced by wave breaking and the plunging waterfall. On the other hand, differences in the number size distribution of aerosols produced by each method could feasibly result from simple scaling of aerosol sizes to the bubble sizes (as is accepted for the jet droplet mechanism; Lewis and Schwartz, 2004), since bubbles from the sintered glass filters did not produce bubbles larger than 1 mm (Prather et al., 2013). If this were the case, the size-resolved composition and mixing state of the SSA produced by each method would be expected to be identical.

3.1.1 Mixing state measurements by ATOFMS

Sea spray aerosol is composed of a mixture of aerosol particles that are chemically distinct, yet fall into several defined “types”; this is referred to as the “external” mixing state. For this intercomparison, the chemical mixing state of 47 927 individual SSA particles generated by controlled breaking waves, plunging waterfall, and sintered glass filters was measured using ATOFMS. The particles were grouped into four types described in detail by Prather et al. (2013): sea salt (SS), sea salt with organic carbon (SS-OC), biological (Bio), and organic-carbon-dominated (OC). A fifth type, labeled “other”, contains Art-2a clusters with minor contributions and/or are attributed to contamination from lab air. A representative dual-polarity mass spectrum for the four main particle types is provided in Fig. 2. The SS type is characterized by prominent ion markers for Na and Cl, with smaller contributions from other inorganic species known to exist in seawater (e.g., K, Ca, Mg). The SS-OC type is characterized

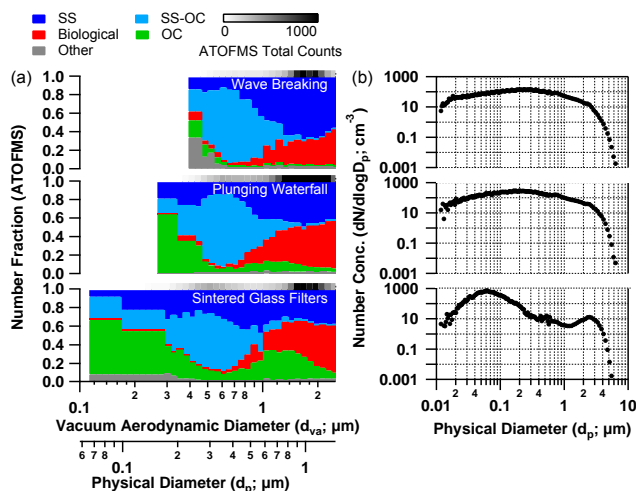


Figure 3. (a) Size-resolved chemical composition of SSA particles measured by ATOFMS for each bubble/aerosol generation method, noted in white text. The vertical scale indicates the number fraction of particles sampled by ATOFMS. The grayscale bar at the top of each panel indicates the number of particles sampled in each size bin. (b) Number size distributions measured by SMPS and APS, corresponding to the data shown in (a). The sintered glass filter method generates a significantly different number size distribution of SSA particles and shows an enhancement in organic-rich particles in the $d_{va} = 0.8\text{--}2\ \mu\text{m}$ range, when compared with the other two generation methods. The second size axis in (a) labeled “Physical Diameter” is provided for comparison with (b), noting that d_{va} is the size metric directly measured by ATOFMS.

by a larger ratio of organic marker ions (CN^- and CNO^- , for example) to chloride. In addition, the contribution of salt ion clusters (NaCl_2^- , MgCl_3^-) is greater in the SS-OC type than in the SS type, and the total absolute intensity of these mass spectra were smaller than for SS. Particles within the SS-OC type had a similar size distribution to SS-OC particles measured by transmission electron microscopy with energy dispersive X-ray analysis (TEM-EDX) in prior studies of nascent SSA produced by wave breaking (Ault et al., 2013; Prather et al., 2013). It is notable that both the SS and SS-OC types have different size distributions and mass spectral signatures, yet both contain markers for organic material (e.g., CN^-). The “biological” (Bio) particle type is characterized by the presence of positive ion markers for Mg, Ca, and transition metals with organic nitrogen, phosphate, and carbohydrate negative ion markers (Pratt et al., 2009; Guasco et al., 2013). The “organic carbon-dominated” (OC) particle type has a large Ca ion marker, with Na also present but to a smaller degree than in the SS and SS-OC types. The negative ion spectrum contains markers for organic nitrogen, carbohydrates, phosphate, and chloride. The presence of Ca in this particle type is in correspondence with CCSEM/EDX analysis presented below and discussed further in Sect. 3.1.2 in the context of the marine organic matter literature.

Particles with $d_{va} > 1\ \mu\text{m}$ were characterized by large number fractions of SS and Bio particles, while particles with $d_{va} < 1\ \mu\text{m}$ were dominated by SS-OC and OC particles. The size-resolved chemical composition of SSA produced by each of the bubble generation methods shown in Fig. 3a is shown alongside the corresponding number size distributions for each method in Fig. 3b. The sampling efficiency for particles with $d_{va} > 1\ \mu\text{m}$ in these experiments was greater than for particles with $d_{va} < 1\ \mu\text{m}$. Therefore, the ability for the ATOFMS to chemically speciate particles at sizes approaching $d_{va} = 0.1\ \mu\text{m}$ was dependent on the number concentration of particles present at that size. The sintered glass filters produced approximately 10-fold higher size-resolved number concentrations than the other two methods (Fig. 3b).

The fraction of OC particles is higher for all measured sizes in the sintered-glass-filter-generated SSA particles compared to wave breaking, whereas the overexpression of OC particles from the plunging waterfall is more moderate. A slightly larger number fraction of biological particles with $d_{va} > 1\ \mu\text{m}$ was also observed in the aerosol generated by plunging waterfall and sintered glass filters, compared with wave breaking. Overall, the fraction of organic and biological SSA particles generated in these experiments increases with a distinct trend: wave breaking < plunging waterfall < sintered glass filters. This trend is especially evident in the supermicron size range, which is also the size range containing the majority of the chemically characterized particles in this study. These ATOFMS results indicate that the size-resolved composition of SSA is directly affected by the physical mechanism of bubble generation.

3.1.2 Elemental composition measurements by electron microscopy

Further single-particle composition measurements were conducted using CCSEM/EDX, which allowed for quantitative chemical analysis of individual particles with $d_{ae} = 0.3\text{--}3\ \mu\text{m}$. Figure 4 compares the enrichment of three different elements ($X = \text{Mg}$, K , and Ca) relative to Na from a collection of individual SSA particles sampled from each of the three generation methods. The comparison is presented as the size-resolved ratio of X/Na for aerosol particles generated using the plunging waterfall (Fig. 4a) and sintered glass filter (Fig. 4b) schemes, divided by the size-resolved X/Na ratio for SSA generated by wave breaking (the reference case). A value of 1 in Fig. 4 means that there is no difference between the X/Na ratio in the SSA generated by the methods being compared. The chemical composition as determined by CCSEM/EDX is very similar across all sizes between the plunging-waterfall and wave-breaking SSA particles. In contrast, SSA generated by the sintered glass filter method shows ratios of Mg/Na , K/Na , and Ca/Na compared to wave-breaking SSA that are much greater than 1 for particles with $d_{ae} = 1\text{--}1.5\ \mu\text{m}$, indicating an enrichment of those ions in supermicron particles. In par-

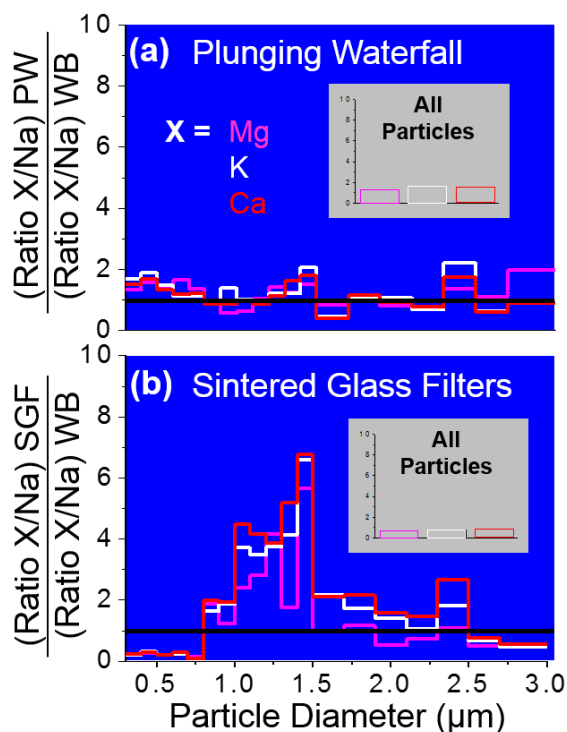


Figure 4. Elemental composition of particles produced via (a) plunging waterfall (PW) and (b) sintered glass filters (SGF), compared to particles produced via wave breaking (WB). The comparison is made using the ratio of the EDX intensities (counts per second) for Mg, K, and Ca referenced to Na in SSA particles. Deviation from unity indicates differences in chemical composition. The number of particles in each size bin can be found in Table 1.

ticles with $d_{ae} < 0.8 \mu\text{m}$, these ionic species are depleted relative to wave-generated SSA, shown by X/Na ratios less than 1. It is important to note that the enhancement and depletion of X/Na ratios relative to wave-generated particles only emerges when their size-resolved composition is measured. Despite the significant deviations from unity observed in the size-resolved particles produced by the sintered glass filter, all three of the elemental ratio comparisons are close to unity when averaged over all particle sizes (Fig. 4, insets). This disparity between the two means of analysis highlights the importance of making size-resolved single-particle measurements due to inherent chemical heterogeneity in an externally mixed aerosol.

Common results from both ATOFMS and CCSEM/EDX analyses are the enrichment of Mg, Ca, and K in SSA generated by sintered glass filters in supermicron particles. ATOFMS measurements show that these cations are mainly localized to OC and biological SSA particles (Fig. 2). The tendency for inorganic cations to coordinate, or strongly associate, with organic and biological material in the ocean and in SSA particles has long been recognized (e.g., Duce and Hoffman, 1976). Divalent cations, such as Mg^{2+} or Ca^{2+} , have the ability to stabilize organic supramolecular struc-

tures (Verdugo, 2012) and coordinate surface-active organic ligands at interfaces (Casillas-Ituarte et al., 2010). Magnesium has been shown to be a good tracer for SSA produced from bacteria-rich seawater (Guasco et al., 2013) and has been observed in aerosol over the ocean in association with biological activity (Gaston et al., 2011). Hence, the enrichment of Ca, Mg, and K in the $1\text{--}1.5 \mu\text{m}$ size range in the CCSEM/EDX analysis is in good agreement with the ATOFMS results, which show an increased fraction of OC and biological particles from the sintered glass filter-generated SSA in this same size range, relative to wave production. The depletion of Mg, K, and Ca in particles with $d_{ae} < 0.8 \mu\text{m}$ observed by CCSEM/EDX suggests that smaller particles have chemical trends opposite those with $d_{ae} > 1 \mu\text{m}$. ATOFMS measurements did not achieve sufficient sampling statistics for detailed comparative analysis. Consequently, any suppression of organic matter in the $d_{ae} = 0.1\text{--}0.8 \mu\text{m}$ size range could not be dually corroborated and should be a topic of future work.

3.1.3 Internal mixing state particles of SS-OC particles

The trend of increasing organic matter enrichment in SSA by plunging waterfall and sintered glass filters compared to wave breaking is not restricted to the variety of particle types observed. Individual types of SSA particles, described in Sect. 3.1.1, often contain mixtures of chemicals within each particle; this is referred to as the “internal” mixing state. The size-resolved fraction of particles containing sea salt mixed with organic carbon (SS-OC) does not appear to change significantly across the three methods (Fig. 3); however, the amount of organic matter in SS-OC particles is different for each bubble generation method. Figure 5 shows the fraction of SS-OC particles that contain mass spectral markers for organic matter, binned by the area under each ion marker peak (an indicator of the quantity of each species in the particle). The fraction of particles that contain NaCl and each organic marker, as well as the organic ion marker peak area, increase with the same pattern as described previously: breaking waves $<$ plunging waterfall $<$ sintered glass filters. Therefore, even within the SS-OC particle type, organic matter is enriched in SSA particles generated by sintered glass filters, while the plunging waterfall produced only a moderate enrichment in organic matter compared to breaking waves.

Morphological details of individual particles were measured using SEM images, examples of which are shown in Fig. 6. The particle cores (which consist mainly of salts) are more rounded in the sintered glass filter sample, compared with the plunging-waterfall and wave-breaking samples. Differences in the morphologies of vacuum-dried SSA particles generated by each method were quantified using a circularity parameter, C , which was calculated for nearly 100 particles with d_{ae} between 0.380 and $2.6 \mu\text{m}$ from each generation

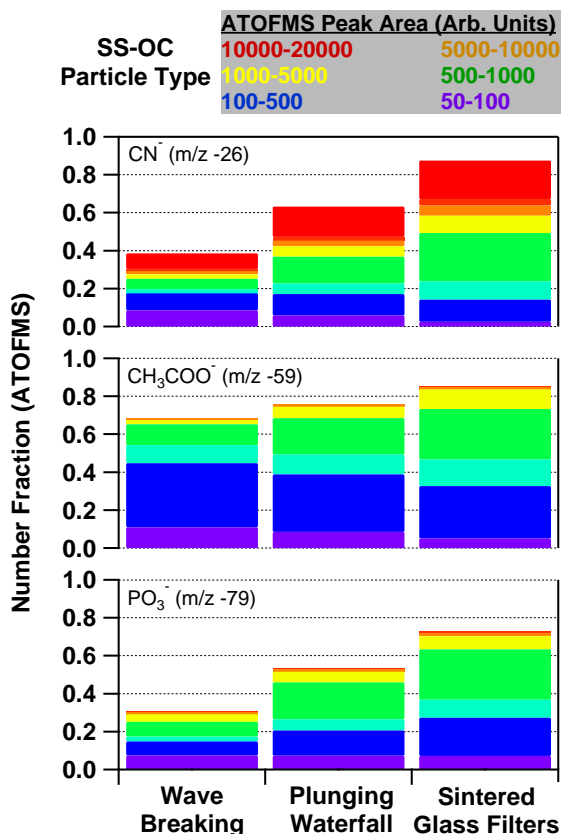


Figure 5. Color-stack plots showing ATOFMS ion markers for organic nitrogen (CN^-), oxygenated organic carbon (CH_3COO^-), and phosphate (PO_3^-), considering only particles composed of an internal mixture of sea salt and organic compounds (SS-OC) all sizes. The vertical axis indicates the number fraction of SS-OC particles whose mass spectrum includes each marker, with the color indicating the peak area of the marker. Notice that, from left to right, a larger fraction of SS-OC particles contain these organic/biomolecule marker ions; the peak area also increases, suggesting that each particle contains more of each chemical species moving from left to right.

method (Eq. 5).

$$C = \frac{4\pi A}{P^2}, \quad (5)$$

where A is the area of an individual particle and P is its perimeter. Particles were counted as either spherical, if C was within 10% of the value for an ideal sphere ($C = 1.00 \pm 0.10$), or cubic, if C was within 10% of the value for an ideal cube ($C = 0.79 \pm 0.08$). Only the “core” of each particle was accounted for in the circularity determination; “shadows” observed around the particles were neglected. It was found that 56% of the SSA particles generated by sintered glass filters were classified as spherical under vacuum, whereas 44% of the SSA particles generated by the plunging waterfall and 32% of the SSA particles generated by wave breaking were classified as spherical. Less

than 1% of the particles measured were characterized as neither spherical nor cubic. For particles that are composed of a mixture of sea salt and organic matter (e.g., SS-OC particles), it has been shown previously that increasing circularity is associated with a greater organic/inorganic volume mixing ratio as cubic crystallization is inhibited (Laskin et al., 2012; Ault et al., 2013). Hence, agreement was observed between the SEM morphology analysis and single-particle analysis by ATOFMS: particles generated by the sintered glass filter method contain more organic matter.

3.2 Continuous foam formation and SSA composition

Natural SSA is mainly produced by whitecaps in the ocean, which are episodic in nature (de Leeuw et al., 2011). The visible white area on the sea surface during and subsequent to a wave-breaking episode is due to the presence of foam, a collection of bubbles floating at the air–sea interface, each separated from the next by a thin liquid film (Bikerman, 1973). Whitecap foam persistence, measured in terms of its exponential decay time, lies mostly in the range of 2–4 s, occasionally extending to times as long as 10 s (Callaghan et al., 2012). The discrete, episodic nature of wave breaking in the natural environment and in wave channel experiments reported here (mimicked also by the duty cycle of the plunging waterfall) is in contrast to the behavior of continuously generated bubble plumes from sintered glass filters. Continuous production of bubbles results in a persistent surface foam, which has been implicated in alterations to SSA production mechanisms (Keene et al., 2007; Tyree et al., 2007) and water uptake properties (King et al., 2012). These observations led to the investigation of the role of time-modulated (or “pulsed”) versus continuous bubble generation on particle production. Using a MART system (Stokes et al., 2013), which produces aerosol through a plunging-waterfall apparatus similar to that implemented in the wave channel inter-comparison experiments described above, the sensitivity of SSA composition to the intermittent nature of the plunging waterfall was tested using both unamended natural seawater ($[\text{TOC}] = 85 \mu\text{M}$) and organic-enriched natural seawater ($[\text{TOC}] = 400 \mu\text{M}$) as described in Sect. 2.2.

3.2.1 Size distributions

The number size distributions of SSA particles were observed to be the nearly identical (within 1σ) between the pulsed and continuous plunging protocols when implemented using unamended natural seawater (Fig. 7a). However, a significant change in the shape of the SSA number size distribution was observed when comparing pulsed and continuous plunging-waterfall protocols in organic-enriched natural seawater (Fig. 7b). The concentration of particles with $d_p < 0.05 \mu\text{m}$ and $d_p > 0.3 \mu\text{m}$ were lower, while concentrations of particles with $d_p = 0.05\text{--}0.125 \mu\text{m}$ were higher for continuous plunging when compared with pulsed plunging.

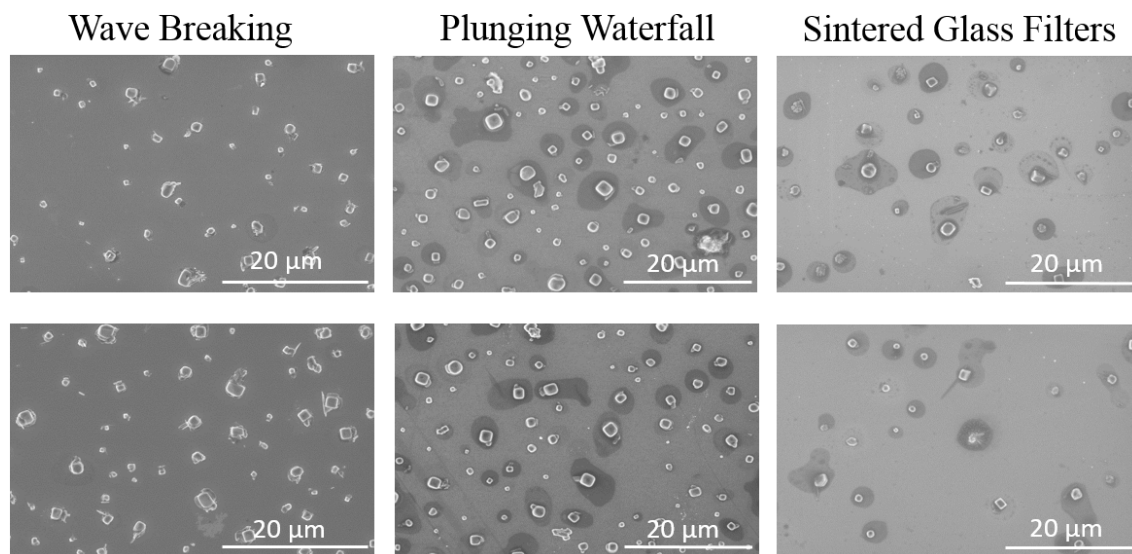


Figure 6. SEM images of particles generated by each of the three laboratory SSA generation mechanisms considered in this study (two images shown for each case). All samples are dried in the vacuum of the SEM during the analysis process. The increased circularity of the particle cores is visible when comparing the sintered glass filter SSA samples to the plunging-waterfall and wave-breaking samples.

ing in the same seawater. Continuous plunging resulted in a tank-wide layer of foam that accumulated on the water surface, whereas surface foam had a patchy character when the plunging waterfall was pulsed at 4 s intervals. The reduced concentration of particles with $d_p > 0.3 \mu\text{m}$ during continuous plunging could be due to weakened jet droplet production, and will be discussed in further detail in Sect. 4.3.

The correlation of changes in the size distribution for $d_p < 0.05 \mu\text{m}$ with particles having $d_p > 0.3 \mu\text{m}$ suggests a physical link between the production mechanism of both large ($d_p > 0.3 \mu\text{m}$) and small ($d_p < 0.05 \mu\text{m}$) SSA particles. The presence of a significant surface foam layer appeared to enhance the production of SSA with $d_p = 0.05\text{--}0.125 \mu\text{m}$, suggesting that cap film breakup plays a significant role in the production of SSA particles in this limited size range. Hence, this type of deliberate foam accumulation experiment is a potentially useful tool for isolating the production mechanism of SSA particles via thin fluid film fragmentation for more detailed studies.

3.2.2 Chemical composition

The chemical composition of SSA produced via continuous and pulsed plunging were indistinguishable when generated from unaltered natural seawater (Fig. 8a, c). However, continuous plunging in organic-enriched natural seawater was associated not only with a change in the SSA particle size distribution (Fig. 7) but also with more organic matter in SSA particles sampled by ATOFMS (Fig. 8b). For instance, the fraction of SS-OC particles measured by ATOFMS that contained organic carbon markers, as well as the area under the organic carbon marker peaks in the SS-OC particles' mass

spectra, was substantially higher in SSA produced by continuous plunging, as compared to pulsed plunging in organic-enriched seawater (Fig. 8). This finding is in general agreement with the response of cloud condensation nuclei activity to foam buildup in a similar type of laboratory experiment utilizing sodium laurate as a surface-active chemical proxy for dissolved organic matter (King et al., 2012). Achieving similar results to those of King et al. (2012) in this study with only 1 % of the concentration of organic material reinforces the critical importance of the naturally complex chemical composition of organic matter used to alter the seawater in this and other recent laboratory SSA experiments (Fuentes et al., 2010a; Moore et al., 2011; Ault et al., 2013; Collins et al., 2013; Prather et al., 2013). The differences observed in SSA composition between the pulsed and continuous plunging modes explored here stress the importance of preserving the transient nature of surface foam inherent to the wave-breaking process in the production of SSA in the laboratory when concentrations of organic matter in the seawater are elevated.

4 Discussion

Direct chemical measurements of laboratory-produced SSA at the single-particle level described in this study indicate that the physical mechanism for bubble generation is inherently linked to particle composition. In this section, a variety of hypotheses are provided for the results of this study, which are discussed in the context of the existing literature. Each concept discussed below is shown schematically in Fig. 9.

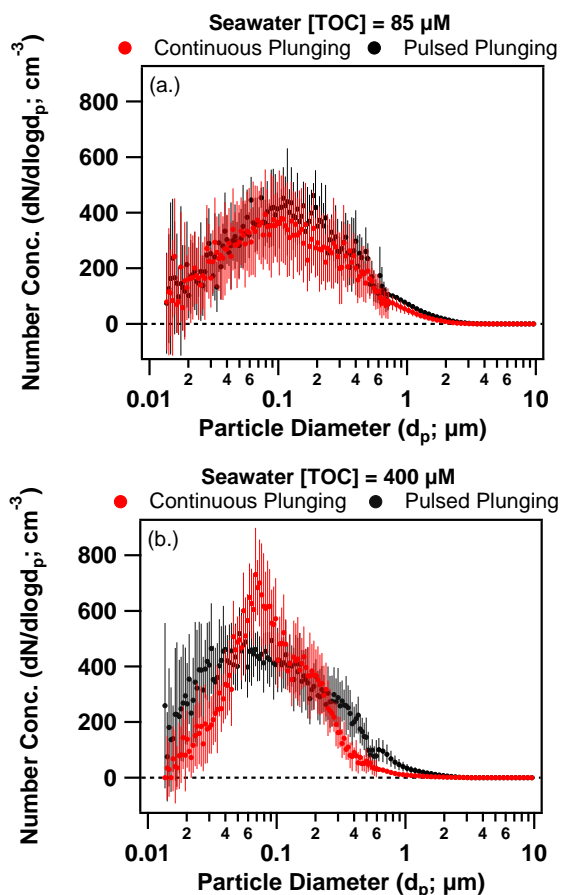


Figure 7. Number size distributions for MART-generated SSA particles using continuous (red) and pulsed (black) plunging-waterfall modes ($\pm 1\sigma$ error bars). The change in the shape of the size distribution is clearly evident between the continuous and pulsed plunging cases when the seawater is enriched with organic matter. Concentrations of particles with $d_p > 0.3$ and $d_p < 0.05$ μm are smaller during continuous plunging, indicating a change in the SSA particle production mechanism due to the overproduction of foam.

4.1 Bubble-mediated surfactant transport

As described in detail above, the size-resolved chemical composition of SSA generated by sintered glass filters contains a larger number fraction of OC particles in the supermicron size range than are found in SSA from breaking waves (Figs. 3 and 4). In addition, particles within the SS-OC type, which do not show as significant a change in number fraction as the OC particles, still undergo an enrichment in organic matter from sintered glass filter production, as compared to SSA from wave breaking and plunging waterfall (Figs. 5 and 6). As discussed by Prather et al. (2013), the bubble size distribution produced by the sintered glass filter setup did not produce bubbles with radius > 1 mm. Subsurface bubbles are known to scavenge surface-active material from the water column and transport the organics to the sea surface (Liss, 1975). Since the efficiency of surfactant scav-

enging by rising bubbles increases as bubble radius decreases (Blanchard, 1975), a greater degree of surfactant scavenging in bubble plumes generated by sintered glass filters is expected as compared to plumes generated by wave breaking or plunging waterfall, assuming the same gas flux rate for all systems, but weighted toward smaller bubbles in the case of the frit. On the whole, the process of surfactant transport toward the air–sea interface would result in the accumulation of organic matter in the sea surface microlayer (SML) (Keene et al., 2007), which is a layer of material at the air–sea interface up to 1 mm thick that is typically highly enriched in dissolved and particulate organic material in the open ocean (Carlson, 1983; Liss and Duce, 1997; Aller et al., 2005; Cunliffe et al., 2011). Some sintered glass filter aerosol generators have been designed to mitigate the over-expression of organics in the SML by continuously refreshing the surface of the seawater subjected to bubbling (Keene et al., 2007; Modini et al., 2010; Bates et al., 2012); this design feature was not explicitly tested in this study. Wurl et al. (2011) show that the SML exists on the ocean surface for wind speeds up to 10 m s^{-1} (global ocean mean wind speed is approximately 6 m s^{-1}), so the existence of the SML is relevant for many instances of wave-induced bubble and foam production. At the same time, dynamic physical processes at the ocean surface can exert control on the thickness and extent of the SML (Cunliffe et al., 2013), so limiting organic matter enrichment at the sea surface is likely important for SSA production studies. Surface-active material is well known to be important to foam lifetime; a recent study discussed its potential influence on whitecap decay time measurements near the east coast of the United States (Callaghan et al., 2012), which was then explicitly tested in recent laboratory studies of bubble decay times (Callaghan et al., 2013; Modini et al., 2013). Still, the extent to which an organic-enriched surface microlayer exists in laboratory-scale SSA generators represents the range of environments in the open ocean has not been explicitly explored. Important considerations for future SSA production studies include surfactant solubility, quantitative analysis of surface/bulk mixing, the dilation, compression and packing of surfactant molecules, along with the already recognized role of subsurface bubble scavenging. As reviewed by de Leeuw et al. (2011), the impact of bubble rise distance could be a contributing factor in organic matter transport from the water column to the air–sea interface (Blanchard and Syzdek, 1972, 1975; Blanchard, 1975), although a recent theoretical assessment conflicts with these results (Fuentes et al., 2010b). While this study did not systematically test the bubble transit distance as a contributing factor in SSA organic matter content, we note that the transit distance of bubbles from breaking waves in this set of experiments (which includes a downward and upward path) was similar to that of the sintered glass filter bubble plume (upward path only), since the penetration depth of the wave was about half the depth of the sintered glass filter setup.

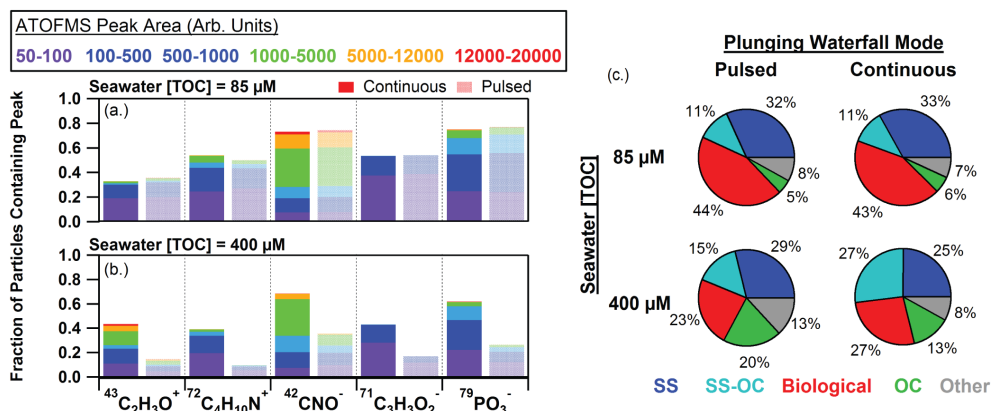


Figure 8. (a, b) Comparison of color-stack plots generated by sampling SSA produced by a plunging waterfall under “continuous” bubble generation versus “pulsed” (4 s on/off) bubble generation. Large differences in SSA composition are observed when seawater organic matter concentrations are high ([TOC] = 400 μM), coinciding with major differences in surface foam accumulation between the generation modes. Only SS-OC particles are considered in (a) and (b). On the right, (c) shows a matrix of pie charts indicating the fractional contribution of each of the particle types to SSA from both pulsed and continuous plunging with both low (85 μM) and high (400 μM) organic matter concentrations in the seawater.

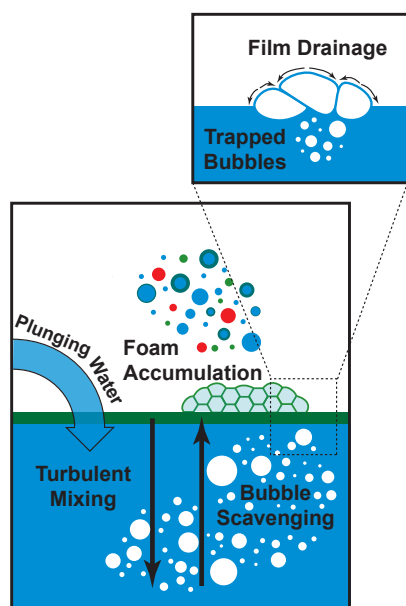


Figure 9. Process diagram of SSA production depicting phenomena described in Sect. 4.

4.2 Surface water mixing

In the breaking wave and plunging-waterfall mechanisms, mixing of sea surface material back into the water column is a phenomenon that counteracts bulk-to-surface transport of surface-active organic matter by the rising bubble plume. Vertical mixing of surface water was observed concurrently with air entrainment and bubble generation in prior wave channel studies of plunging breakers (Rapp and Melville, 1990), and is expected to translate to bubble entrainment by

the plunging waterfall due to the similarity of the bubble formation processes between these two SSA generation methods. The lack of mixing of the organic-enriched SML back into the water column, as is likely the case for sintered glass filters due to the lack of surface penetration, could also contribute to the observed enhancements of organic matter in SSA relative to wave breaking, as described above. The results provided in this study suggest that generating aerosol using a technique where surface-active organic material is mixed back into the water column provides a similar mitigation of organic enrichment in the SML. Based on this explanation, the composition of SSA from the plunging waterfall suggests that the surface water mixing regime lies between that of wave breaking and sintered glass filters.

4.3 Foam layer accumulation

The impact of a layer of accumulated, persistent foam on SSA production was investigated by comparing the size distribution and composition of SSA produced from the plunging waterfall in pulsed and continuous operation. The two operation modes produced SSA differently only while the seawater was enriched with organic matter ([TOC] = 400 μM), and a persistent layer of foam was observed on the water surface.

The transient nature of surface foam in natural wave breaking has been discussed in the context of a continuous plunging water jet technique (Fuentes et al., 2010b), where the bubble plume and foam on the water surface is allowed to decay as it moves away from the jet impingement location. The continuous production of bubbles that have a size distribution closely mimicking that within oceanic breaking waves in an experiment utilizing a plunging water technique may closely approximate wave-breaking SSA composition at mean TOC

concentration (60–85 μM), but not when using seawater that is enriched with organic matter (Figs. 7 and 8). Addition of soluble surfactants to salt water is known to increase bubble lifetime (Modini et al., 2013), and can lead to more persistent whitecap foam following a breaking wave event (Callaghan et al., 2013). The properties of persistent foam are temporally dynamic. Foam cell size distributions are subject to fluid film rupture, which gives rise to processes which can both coarsen the foam by coalescence (e.g., Colin, 2012) and cause foam fining through daughter bubble production (Bird et al., 2010). Direct measurements of aerosol production with quantitative measurements of foam properties have not been shown in the literature to date; however, results shown in Sect. 3.2, along with those reported by King et al. (2012), indicate that foam properties can exert a significant influence on the physical and chemical characteristics of SSA.

As bubbles age on the seawater surface, the cap films are known to drain and thin; these types of time-dependent processes have been shown to influence aerosol production in single bubble experiments (Modini et al., 2013). In this study, the production of SSA particles from persistent foam that is greater than one bubble layer thick (continuous plunging, high [TOC]) was associated with increased organic matter in the particles compared to SSA generated from the bursting of bubbles while a less pronounced foam layer existed (pulsed plunging, low [TOC]; Fig. 8). We hypothesize that foam bubble bursting could (1) preferentially produce particles that are more enriched in organic matter than free bubbles bursting at the air–sea interface due to bubble cap film draining and thinning processes, and/or (2) droplets produced by the bursting of thin fluid films (film drops) are inherently enhanced in organics as a result of their production mechanism. While these hypotheses are not mutually exclusive and the former would require further detailed measurements, the latter concept is supported by the coincidence of the accepted film droplet size distribution (Lewis and Schwartz, 2004; de Leeuw et al., 2011) and the size-resolved enhancement of organic matter in nascent, submicron SSA particles (e.g., Keene et al., 2007; Facchini et al., 2008; Gantt and Meskhidze, 2013; Prather et al., 2013).

The existence of a layer of foam on the seawater surface was also associated with a change in the shape of the SSA size distribution (Fig. 7). The low concentrations of SSA particles with $d_p > 0.3 \mu\text{m}$ is perhaps indicative of reduced aerosol production by the jet droplet mechanism, based on particle size (Lewis and Schwartz, 2004; de Leeuw et al., 2011). The existence of the foam layer on the seawater surface may be capable of prohibiting or curtailing jet droplet production by assimilating rising bubbles into the foam layer prior to rupture. The mechanism for jet droplet formation via rapid retraction of surface water within the cavity (Lewis and Schwartz, 2004) of a bursting bubble is likely to be impossible in the absence of a continuous liquid phase beneath the bursting bubble, as in a foam that is greater than one bubble layer thick. In addition, we suggest that jet droplets that

may have formed beneath the foam layer would have been sequestered by the overlying foam, causing a reduction in jet droplet introduction to the air above the foam (Fig. 9, inset). In either case, the reduced formation of particles with $d_p > 0.3 \mu\text{m}$ when a persistent layer of foam was observed clearly links a change in SSA production with surface foam accumulation.

5 Conclusions

Due to uncertainties in the projections of global climate that stem from natural aerosol sources, detailed studies of SSA in controlled environments approximating preindustrial conditions are of great importance (Menon et al., 2002; Ghan et al., 2013; Tsigaridis et al., 2013). At the same time, controlled laboratory studies that utilize physicochemically accurate SSA production taking into account realistic biogeochemical systems are critical for developing an understanding of natural geochemical and geophysical interactions that influence the global climate system. It has been shown in this study that the composition of laboratory-generated SSA was inherently sensitive to the physicochemical environment (controlled by the bubble production mechanism) in which bubbles were generated and allowed to burst. In addition, the pulsed or periodic nature of bubble production was important in controlling the transfer of organic matter to SSA via surface foam accumulation when high concentrations of organic matter are present in the seawater. Based on the results presented in Sect. 3.2, it is also shown that SSA production studies with accumulated foam layers can be a useful tool in enhancing the formation of SSA via thin fluid film rupture.

When compared with wave breaking and plunging waterfall in this study, the sintered glass filter apparatus produced a different bubble size distribution and different surface foam accumulation properties. The modal diameter and shape of the sintered glass filter aerosol number size distribution are clearly distinguishable from the plunging-waterfall and wave-breaking size distributions. Size-resolved, single-particle chemical composition measurements of SSA particles produced by the sintered glass filters showed a larger contribution of OC from supermicron particles compared to those from both plunging waterfall and wave breaking. While it has been established that the similarity of the bubble size distribution in laboratory SSA generators to that in the open ocean is an important factor (Fuentes et al., 2010b; Prather et al., 2013), these authors suspect that turbulent mixing of the organic-enriched surface microlayer back into the water column by the breaking waves and plunging waterfall, and perceived lack thereof by the sintered glass filters (as implemented in this study), may play a role in the results presented in the intercomparison portion of this study (Sect. 3.1). The natural conformity of the physical and chemical environment for bubble generation and bursting are critical for an accurate reproduction of SSA generation in the laboratory. It is

possible that a careful redesign of the sintered glass filter setup used in this study could allow for SSA production that more closely matches the wave-breaking method described in this study. In general, new SSA generation schemes should not only replicate the bubble size distribution of open ocean waves but also the inherently turbulent and discrete nature of the wave-breaking process.

The correspondence of similarities and differences in both the size distribution and chemical composition of SSA particles generated by the methods explored in this study stresses the inherent coupling between the SSA production mechanism and its composition. Hence, this study indicates that the similarity of the number size distribution of laboratory-generated SSA to the best available reference (e.g., laboratory breaking waves) can be utilized as a first-order check on SSA composition. This study takes important steps toward bringing the marine environment into the laboratory by evaluating the natural fidelity of the starting material utilized for many chemical and physical studies of SSA particles through a critical intercomparison of various SSA generation mechanisms.

Acknowledgements. This study was funded through the Center for Aerosol Impacts on Climate and the Environment (CAICE), a National Science Foundation Center for Chemical Innovation (CHE-1305427). Dave Aglietti, John Lyons, Paul Harvey, and Charles Coughran of the Scripps Institution of Oceanography Hydraulics Laboratory provided valuable assistance and expertise to the technical development of the facilities used in this study. Total organic carbon analysis reported herein was performed by M. Porrachia at Scripps Institution of Oceanography. The referees of this manuscript are acknowledged for their thorough, thoughtful, and constructive criticism. Any opinions, findings, conclusions, or recommendations expressed in this material are those of the authors and do not necessarily reflect the views of the National Science Foundation.

Edited by: P. Herckes

References

- Aller, J. Y., Kuznetsova, M. R., Jahns, C. J., and Kemp, P. F.: The sea surface microlayer as a source of viral and bacterial enrichment in marine aerosols, *J. Aerosol. Sci.*, 36, 801–812, doi:10.1016/j.jaerosci.2004.10.012, 2005.
- Andreae, M. O. and Crutzen, P. J.: Atmospheric aerosols: Biogeochemical sources and role in atmospheric chemistry, *Science*, 276, 1052–1058, doi:10.1126/science.276.5315.1052, 1997.
- Andreae, M. O. and Rosenfeld, D.: Aerosol-cloud-precipitation interactions. Part 1. The nature and sources of cloud-active aerosols, *Earth-Sci. Rev.*, 89, 13–41, doi:10.1016/j.earscirev.2008.03.001, 2008.
- Ault, A. P., Moffet, R. C., Baltrusaitis, J., Collins, D. B., Ruppel, M. J., Cuadra-Rodriguez, L. A., Zhao, D. F., Guasco, T. L., Ebben, C. J., Geiger, F. M., Bertram, T. H., Prather, K. A., and Grassian, V. H.: Size-Dependent Changes in Sea Spray Aerosol Composition and Properties with Different Seawater Conditions, *Environ. Sci. Technol.*, 47, 5603–5612, doi:10.1021/Es400416g, 2013.
- Azam, F. and Malfatti, F.: Microbial structuring of marine ecosystems, *Nat. Rev. Microbiol.*, 5, 782–791, doi:10.1038/Nrmicro1747, 2007.
- Bates, T. S., Quinn, P. K., Frossard, A. A., Russell, L. M., Hakala, J., Petaja, T., Kulmala, M., Covert, D. S., Cappa, C. D., Li, S. M., Hayden, K. L., Nuaaman, I., McLaren, R., Massoli, P., Canagaratna, M. R., Onasch, T. B., Sueper, D., Worsnop, D. R., and Keene, W. C.: Measurements of ocean derived aerosol off the coast of California, *J. Geophys. Res.-Atmos.*, 117, D00v15, doi:10.1029/2012jd017588, 2012.
- Bikerman, J. J.: *Foams*, Applied Physics and Engineering, 10, Springer Verlag, New York, 337 pp., 1973.
- Bird, J. C., de Ruiter, R., Courbin, L., and Stone, H. A.: Daughter bubble cascades produced by folding of ruptured thin films, *Nature*, 465, 759–762, doi:10.1038/Nature09069, 2010.
- Blanchard, D. C.: Sea-to-Air Transport of Surface Active Material, *Science*, 146, 396–397, 1964.
- Blanchard, D. C.: Bubble Scavenging and Water-to-Air Transfer of Organic Material in Sea, *Adv. Chem. Ser.*, 360–387, 1975.
- Blanchard, D. C. and Syzdek, L. D.: Concentration of Bacteria in Jet Drops from Bursting Bubbles, *J. Geophys. Res.*, 77, 5087, doi:10.1029/Jc077i027p05087, 1972.
- Blanchard, D. C. and Syzdek, L. D.: Electrostatic Collection of Jet and Film Drops, *Limnol. Oceanogr.*, 20, 762–774, 1975.
- Blanchard, D. C. and Woodcock, A. H.: Bubble Formation and Modification in the Sea and Its Meteorological Significance, *Tellus*, 9, 145–158, 1957.
- Brown, S. S. and Stutz, J.: Nighttime radical observations and chemistry, *Chem. Soc. Rev.*, 41, 6405–6447, doi:10.1039/c2cs35181a, 2012.
- Callaghan, A. H., Deane, G. B., Stokes, M. D., and Ward, B.: Observed variation in the decay time of oceanic whitecap foam, *J. Geophys. Res.-Oceans*, 117, C09015, doi:10.1029/2012jc008147, 2012.
- Callaghan, A. H., Deane, G. B., and Stokes, M. D.: Two Regimes of Laboratory Whitecap Foam Decay: Bubble-Plume Controlled and Surfactant Stabilized, *J. Phys. Oceanogr.*, 43, 1114–1126, doi:10.1175/Jpo-D-12-0148.1, 2013.
- Carlson, D. J.: Dissolved Organic Materials in Surface Microlayers – Temporal and Spatial Variability and Relation to Sea State, *Limnol. Oceanogr.*, 28, 415–431, 1983.
- Carslaw, K. S., Lee, L. A., Reddington, C. L., Pringle, K. J., Rap, A., Forster, P. M., Mann, G. W., Spracklen, D. V., Woodhouse, M. T., Regayre, L. A., and Pierce, J. R.: Large contribution of natural aerosols to uncertainty in indirect forcing, *Nature*, 503, 67–71, doi:10.1038/nature12674, 2013.
- Casillas-Ituarte, N. N., Callahan, K. M., Tang, C. Y., Chen, X. K., Roeselova, M., Tobias, D. J., and Allen, H. C.: Surface organization of aqueous MgCl₂ and application to atmospheric marine aerosol chemistry, *P. Natl. Acad. Sci. USA*, 107, 6616–6621, doi:10.1073/pnas.0912322107, 2010.
- Charlson, R. J., Schwartz, S. E., Hales, J. M., Cess, R. D., Coakley, J. A., Hansen, J. E., and Hofmann, D. J.: Climate Forcing by Anthropogenic Aerosols, *Science*, 255, 423–430, doi:10.1126/science.255.5043.423, 1992.
- Cloke, J., McKay, W. A., and Liss, P. S.: Laboratory Investigations into the Effect of Marine Organic Material on the Sea-Salt

- Aerosol Generated by Bubble Bursting, *Mar. Chem.*, 34, 77–95, doi:10.1016/0304-4203(91)90015-O, 1991.
- Colin, A.: Coalescence in Foams, in: *Foam Engineering: Fundamentals and Applications*, edited by: Stevenson, P., John Wiley & Sons, Ltd., Chichester, UK, 75–90, 2012.
- Collins, D. B., Ault, A. P., Moffet, R. C., Ruppel, M. J., Cuadra-Rodriguez, L. A., Guasco, T. L., Corrigan, C. E., Pedler, B. E., Azam, F., Aluwihare, L. I., Bertram, T. H., Roberts, G. C., Grassian, V. H., and Prather, K. A.: Impact of marine biogeochemistry on the chemical mixing state and cloud forming ability of nascent sea spray aerosol, *J. Geophys. Res.-Atmos.*, 118, 8553–8565, doi:10.1002/Jgrd.50598, 2013.
- Cunliffe, M., Upstill-Goddard, R. C., and Murrell, J. C.: Microbiology of aquatic surface microlayers, *FEMS Microbiol. Rev.*, 35, 233–246, doi:10.1111/J.1574-6976.2010.00246.X, 2011.
- Cunliffe, M., Engel, A., Frka, S., Gasparovic, B., Guitart, C., Murrell, J. C., Salter, M., Stolle, C., Upstill-Goddard, R., and Wurl, O.: Sea surface microlayers: A unified physicochemical and biological perspective of the air-ocean interface, *Prog. Oceanogr.*, 109, 104–116, doi:10.1016/j.pocean.2012.08.004, 2013.
- Deane, G. B. and Stokes, M. D.: Scale dependence of bubble creation mechanisms in breaking waves, *Nature*, 418, 839–844, doi:10.1038/nature00967, 2002.
- DeCarlo, P. F., Slowik, J. G., Worsnop, D. R., Davidovits, P., and Jimenez, J. L.: Particle morphology and density characterization by combined mobility and aerodynamic diameter measurements. Part 1: Theory, *Aerosol Sci. Tech.*, 38, 1185–1205, doi:10.1080/027868290903907, 2004.
- de Leeuw, G., Andreas, E. L., Anguelova, M. D., Fairall, C. W., Lewis, E. R., O'Dowd, C., Schulz, M., and Schwartz, S. E.: Production Flux of Sea Spray Aerosol, *Rev. Geophys.*, 49, Rg2001, doi:10.1029/2010rg000349, 2011.
- Duce, R. A. and Hoffman, E. J.: Chemical Fractionation at Air-Sea Interface, *Annu. Rev. Earth Pl. Sc.*, 4, 187–228, doi:10.1146/annurev.ea.04.050176.001155, 1976.
- Facchini, M. C., Rinaldi, M., Decesari, S., Carbone, C., Finessi, E., Mircea, M., Fuzzi, S., Ceburnis, D., Flanagan, R., Nilsson, E. D., de Leeuw, G., Martino, M., Woeltjen, J., and O'Dowd, C. D.: Primary submicron marine aerosol dominated by insoluble organic colloids and aggregates, *Geophys. Res. Lett.*, 35, L17814, doi:10.1029/2008gl034210, 2008.
- Fuentes, E., Coe, H., Green, D., de Leeuw, G., and McFiggans, G.: On the impacts of phytoplankton-derived organic matter on the properties of the primary marine aerosol – Part 1: Source fluxes, *Atmos. Chem. Phys.*, 10, 9295–9317, doi:10.5194/acp-10-9295-2010, 2010a.
- Fuentes, E., Coe, H., Green, D., de Leeuw, G., and McFiggans, G.: Laboratory-generated primary marine aerosol via bubble-bursting and atomization, *Atmos. Meas. Tech.*, 3, 141–162, doi:10.5194/amt-3-141-2010, 2010b.
- Gantt, B. and Meskhidze, N.: The physical and chemical characteristics of marine primary organic aerosol: a review, *Atmos. Chem. Phys.*, 13, 3979–3996, doi:10.5194/acp-13-3979-2013, 2013.
- Gard, E., Mayer, J. E., Morrical, B. D., Dienes, T., Ferguson, D. P., and Prather, K. A.: Real-time analysis of individual atmospheric aerosol particles: Design and performance of a portable ATOFMS, *Anal. Chem.*, 69, 4083–4091, doi:10.1021/ac970540n, 1997.
- Gaston, C. J., Furutani, H., Guazzotti, S. A., Coffee, K. R., Bates, T., Quinn, P., Aluwihare, L. I., Mitchell, B. G., and Prather, K. A.: Unique ocean-derived particles serve as a proxy for changes in ocean chemistry, *J. Geophys. Res.-Atmos.*, 116, D18310, doi:10.1029/2010JD015289, 2011.
- Ghan, S. J., Smith, S. J., Wang, M. H., Zhang, K., Pringle, K. J., Carslaw, K. S., Pierce, J. R., Bauer, S. E., and Adams, P. J.: A simple model of global aerosol indirect effects, *J. Geophys. Res.-Atmos.*, 118, 6688–6707, doi:10.1002/jgrd.50567, 2013.
- Guasco, T. L., Cuadra-Rodriguez, L. A., Pedler, B. E., Ault, A. P., Collins, D. B., Zhao, D., Kim, M. J., Ruppel, M. J., Wilson, S. C., Pomeroy, R. S., Grassian, V. H., Azam, F., Bertram, T. H., and Prather, K. A.: Transition metal associations with primary biological particles in sea spray aerosol generated in a wave channel, *Environ. Sci. Technol.*, 48, 1324–1333, doi:10.1021/es403203d, 2013.
- Hultin, K. A. H., Nilsson, E. D., Krejci, R., Martensson, E. M., Ehn, M., Hagstrom, A., and de Leeuw, G.: In situ laboratory sea spray production during the Marine Aerosol Production 2006 cruise on the northeastern Atlantic Ocean, *J. Geophys. Res.-Atmos.*, 115, D06201, doi:10.1029/2009jd012522, 2010.
- Keene, W. C., Maring, H., Maben, J. R., Kieber, D. J., Pszenny, A. A. P., Dahl, E. E., Izaguirre, M. A., Davis, A. J., Long, M. S., Zhou, X. L., Smoydzin, L., and Sander, R.: Chemical and physical characteristics of nascent aerosols produced by bursting bubbles at a model air-sea interface, *J. Geophys. Res.-Atmos.*, 112, D21202, doi:10.1029/2007jd008464, 2007.
- King, S. M., Butcher, A. C., Rosenorn, T., Lieke, K. I., de Leeuw, G., Nilsson, D., and Bilde, M.: Investigating primary marine aerosol properties: CCN activity of sea salt and mixed inorganic-organic particles, *Environ. Sci. Technol.*, 46, 10405–10412, doi:10.1021/es300574u, 2012.
- Laskin, A., Moffet, R. C., Gilles, M. K., Fast, J. D., Zaveri, R. A., Wang, B. B., Nigge, P., and Shutthanandan, J.: Tropospheric chemistry of internally mixed sea salt and organic particles: Surprising reactivity of NaCl with weak organic acids, *J. Geophys. Res.-Atmos.*, 117, D15302, doi:10.1029/2012jd017743, 2012.
- Lewis, E. R. and Schwartz, S. E.: *Sea Salt Aerosol Production: Mechanisms, Methods, Measurements, and Models – A Critical Review*, Geophysical Monograph 152, American Geophysical Union, Washington, DC, 413 pp., 2004.
- Liss, P. S.: Chemistry of the sea surface microlayer, in: *Chemical Oceanography*, edited by: Riley, J. P. and Skirrow, G., Academic Press, London, 193–244, 1975.
- Liss, P. S. and Duce, R. A.: *The Sea Surface and Global Change*, Cambridge University Press, New York, 519 pp., 1997.
- Lohmann, U. and Feichter, J.: Global indirect aerosol effects: a review, *Atmos. Chem. Phys.*, 5, 715–737, doi:10.5194/acp-5-715-2005, 2005.
- Menon, S., Del Genio, A. D., Koch, D., and Tselioudis, G.: GCM Simulations of the aerosol indirect effect: Sensitivity to cloud parameterization and aerosol burden, *J. Atmos. Sci.*, 59, 692–713, 2002.
- Modini, R. L., Harris, B., and Ristovski, Z. D.: The organic fraction of bubble-generated, accumulation mode Sea Spray Aerosol (SSA), *Atmos. Chem. Phys.*, 10, 2867–2877, doi:10.5194/acp-10-2867-2010, 2010.
- Modini, R. L., Russell, L. M., Deane, G. B., and Stokes, M. D.: Effect of soluble surfactant on bubble persistence and

- bubble-produced aerosol particles, *J. Geophys. Res.-Atmos.*, 118, 1388–1400, doi:10.1002/Jgrd.50186, 2013.
- Moore, M. J. K., Furutani, H., Roberts, G. C., Moffet, R. C., Gilles, M. K., Palenik, B., and Prather, K. A.: Effect of organic compounds on cloud condensation nuclei (CCN) activity of sea spray aerosol produced by bubble bursting, *Atmos. Environ.*, 45, 7462–7469, doi:10.1016/j.atmosenv.2011.04.034, 2011.
- Novakov, T., Corrigan, C. E., Penner, J. E., Chuang, C. C., Rosario, O., and Bracero, O. L. M.: Organic aerosols in the Caribbean trade winds: A natural source?, *J. Geophys. Res.-Atmos.*, 102, 21307–21313, doi:10.1029/97jd01487, 1997.
- O'Brien, R. E., Neu, A., Epstein, S. A., MacMillan, A. C., Wang, B., Kelly, S. T., Nizkorodov, S. A., Laskin, A., Moffet, R. C., and Gilles, M. K.: Physical properties of ambient and laboratory-generated secondary organic aerosol, *Geophys. Res. Lett.*, 41, 4347–4353, doi:10.1002/2014GL060219, 2014.
- O'Dowd, C. D., Facchini, M. C., Cavalli, F., Ceburnis, D., Mircea, M., Decesari, S., Fuzzi, S., Yoon, Y. J., and Putaud, J. P.: Biogenically driven organic contribution to marine aerosol, *Nature*, 431, 676–680, doi:10.1038/nature02959, 2004.
- Ogawa, H., Amagai, Y., Koike, I., Kaiser, K., and Benner, R.: Production of refractory dissolved organic matter by bacteria, *Science*, 292, 917–920, doi:10.1126/science.1057627, 2001.
- Park, J. Y., Lim, S., and Park, K.: Mixing State of Submicrometer Sea Spray Particles Enriched by Insoluble Species in Bubble-Bursting Experiments, *J. Atmos. Ocean. Tech.*, 31, 93–104, doi:10.1175/Jtech-D-13-00086.1, 2014.
- Pomeroy, L. R., Williams, P. J. I., Azam, F., and Hobbie, J. E.: The Microbial Loop, *Oceanography*, 20, 28–33, 2007.
- Prather, K. A., Bertram, T. H., Grassian, V. H., Deane, G. B., Stokes, M. D., DeMott, P. J., Aluwihare, L. I., Palenik, B. P., Azam, F., Seinfeld, J. H., Moffet, R. C., Molina, M. J., Cappa, C. D., Geiger, F. M., Roberts, G. C., Russell, L. M., Ault, A. P., Baltrusaitis, J., Collins, D. B., Corrigan, C. E., Cuadra-Rodriguez, L. A., Ebben, C. J., Forestieri, S. D., Guasco, T. L., Hersey, S. P., Kim, M. J., Lambert, W. F., Modini, R. L., Mui, W., Pedler, B. E., Ruppel, M. J., Ryder, O. S., Schoepp, N. G., Sullivan, R. C., and Zhao, D. F.: Bringing the ocean into the laboratory to probe the chemical complexity of sea spray aerosol, *P. Natl. Acad. Sci. USA*, 110, 7550–7555, doi:10.1073/pnas.1300262110, 2013.
- Pratt, K. A., DeMott, P. J., French, J. R., Wang, Z., Westphal, D. L., Heymsfield, A. J., Twohy, C. H., Prenni, A. J., and Prather, K. A.: In situ detection of biological particles in cloud ice-crystals, *Nat. Geosci.*, 2, 397–400, doi:10.1038/Ngeo521, 2009.
- Quinn, P. K. and Bates, T. S.: The case against climate regulation via oceanic phytoplankton sulphur emissions, *Nature*, 480, 51–56, doi:10.1038/nature10580, 2011.
- Quinn, P. K., Bates, T. S., Schultz, K. S., Coffman, D. J., Frossard, A. A., Russell, L. M., Keene, W. C., and Kieber, D. J.: Contribution of sea surface carbon pool to organic matter enrichment in sea spray aerosol, *Nat. Geosci.*, 7, 228–232, doi:10.1038/ngeo2092, 2014.
- Ramanathan, V., Crutzen, P. J., Kiehl, J. T., and Rosenfeld, D.: Atmosphere – Aerosols, climate, and the hydrological cycle, *Science*, 294, 2119–2124, doi:10.1126/science.1064034, 2001.
- Rapp, R. J. and Melville, W. K.: Laboratory Measurements of Deep-Water Breaking Waves, *Philos. T. Roy. Soc. A*, 331, 735–800, doi:10.1098/rsta.1990.0098, 1990.
- Sciare, J., Favez, O., Sarda-Estève, R., Oikonomou, K., Cachier, H., and Kazan, V.: Long-term observations of carbonaceous aerosols in the Austral Ocean atmosphere: Evidence of a biogenic marine organic source, *J. Geophys. Res.-Atmos.*, 114, D15302, doi:10.1029/2009jd011998, 2009.
- Sellegri, K., O'Dowd, C. D., Yoon, Y. J., Jennings, S. G., and de Leeuw, G.: Surfactants and submicron sea spray generation, *J. Geophys. Res.-Atmos.*, 111, D22215, doi:10.1029/2005jd006658, 2006.
- Shank, L. M., Howell, S., Clarke, A. D., Freitag, S., Brekhovskikh, V., Kapustin, V., McNaughton, C., Campos, T., and Wood, R.: Organic matter and non-refractory aerosol over the remote Southeast Pacific: oceanic and combustion sources, *Atmos. Chem. Phys.*, 12, 557–576, doi:10.5194/acp-12-557-2012, 2012.
- Song, X. H., Hopke, P. K., Fergenson, D. P., and Prather, K. A.: Classification of single particles analyzed by ATOFMS using an artificial neural network, ART-2A, *Anal. Chem.*, 71, 860–865, 1999.
- Sorooshian, A., Padro, L. T., Nenes, A., Feingold, G., McComiskey, A., Hersey, S. P., Gates, H., Jonsson, H. H., Miller, S. D., Stephens, G. L., Flagan, R. C., and Seinfeld, J. H.: On the link between ocean biota emissions, aerosol, and maritime clouds: Airborne, ground, and satellite measurements off the coast of California, *Global Biogeochem. Cy.*, 23, GB4007, doi:10.1029/2009gb003464, 2009.
- Stokes, M. D., Deane, G. B., Prather, K., Bertram, T. H., Ruppel, M. J., Ryder, O. S., Brady, J. M., and Zhao, D.: A Marine Aerosol Reference Tank system as a breaking wave analogue for the production of foam and sea-spray aerosols, *Atmos. Meas. Tech.*, 6, 1085–1094, doi:10.5194/amt-6-1085-2013, 2013.
- Su, Y. X., Sipin, M. F., Furutani, H., and Prather, K. A.: Development and characterization of an aerosol time-of-flight mass spectrometer with increased detection efficiency, *Anal. Chem.*, 76, 712–719, doi:10.1021/ac034797z, 2004.
- Teeling, H., Fuchs, B. M., Becher, D., Klockow, C., Gardebrecht, A., Bennis, C. M., Kassabgy, M., Huang, S. X., Mann, A. J., Waldmann, J., Weber, M., Klindworth, A., Otto, A., Lange, J., Bernhardt, J., Reinsch, C., Hecker, M., Peplies, J., Bockelmann, F. D., Callies, U., Gerdt, G., Wichels, A., Wiltshire, K. H., Glockner, F. O., Schweder, T., and Amann, R.: Substrate-Controlled Succession of Marine Bacterioplankton Populations Induced by a Phytoplankton Bloom, *Science*, 336, 608–611, doi:10.1126/science.1218344, 2012.
- Tsigaridis, K., Koch, D., and Menon, S.: Uncertainties and importance of sea spray composition on aerosol direct and indirect effects, *J. Geophys. Res.-Atmos.*, 118, 220–235, doi:10.1029/2012jd018165, 2013.
- Tyree, C. A., Hellion, V. M., Alexandrova, O. A., and Allen, J. O.: Foam droplets generated from natural and artificial seawaters, *J. Geophys. Res.-Atmos.*, 112, D12204, doi:10.1029/2006jd007729, 2007.
- Verdugo, P.: Marine Microgels, *Annu. Rev. Mar. Sci.*, 4, 375–400, doi:10.1146/annurev-marine-120709-142759, 2012.
- Wise, M. E., Freney, E. J., Tyree, C. A., Allen, J. O., Martin, S. T., Russell, L. M., and Buseck, P. R.: Hygroscopic behavior and liquid-layer composition of aerosol particles generated from natural and artificial seawater, *J. Geophys. Res.-Atmos.*, 114, D03201, doi:10.1029/2008jd010449, 2009.

- Wurl, O., Wurl, E., Miller, L., Johnson, K., and Vagle, S.: Formation and global distribution of sea-surface microlayers, *Biogeosciences*, 8, 121–135, doi:10.5194/bg-8-121-2011, 2011.
- Yoon, Y. J., Ceburnis, D., Cavalli, F., Jourdan, O., Putaud, J. P., Facchini, M. C., Decesari, S., Fuzzi, S., Sellegri, K., Jennings, S. G., and O'Dowd, C. D.: Seasonal characteristics of the physicochemical properties of North Atlantic marine atmospheric aerosols, *J. Geophys. Res.-Atmos.*, 112, D04206, doi:10.1029/2005jd007044, 2007.
- Zábori, J., Matisāns, M., Krejci, R., Nilsson, E. D., and Ström, J.: Artificial primary marine aerosol production: a laboratory study with varying water temperature, salinity, and succinic acid concentration, *Atmos. Chem. Phys.*, 12, 10709–10724, doi:10.5194/acp-12-10709-2012, 2012.
- Zelenyuk, A., Imre, D., Cuadra-Rodriguez, L. A., and Ellison, B.: Measurements and interpretation of the effect of a soluble organic surfactant on the density, shape and water uptake of hygroscopic particles, *J. Aerosol Sci.*, 38, 903–923, doi:10.1016/j.jaerosci.2007.06.006, 2007.